

## ABSTRACT

### A SEARCH FOR EXTRASOLAR PLANETS USING ECHOES PRODUCED IN FLARE EVENTS

A detection technique for searching for extrasolar planets using stellar flare events is explored, including a discussion of potential benefits, potential problems, and limitations of the method. The detection technique analyses the observed time verses intensity profile of a star's energetic flare to determine possible existence of a nearby planet. When measuring the pulse of light produced by a flare, the detection of an echo may indicate the presence of a nearby reflective surface. The flare, acting much like the pulse in a radar system, would give information about the location and relative size of the planet. This method of detection has the potential to give science a new tool with which to further humankind's understanding of planetary systems.

Randal Eugene Clark  
May 2009



A SEARCH FOR EXTRASOLAR PLANETS USING  
ECHOES PRODUCED IN FLARE EVENTS

by  
Randal Eugene Clark

A thesis  
submitted in partial  
fulfillment of the requirements for the degree of  
Master of Science in Physics  
in the College of Science and Mathematics  
California State University, Fresno  
May 2009



APPROVED

For the Department of Physics:

We, the undersigned, certify that the thesis of the following student meets the required standards of scholarship, format, and style of the university and the student's graduate degree program for the awarding of the master's degree.

\_\_\_\_\_  
Randal Eugene Clark  
Thesis Author

\_\_\_\_\_  
Fred Ringwald (Chair) Physics

\_\_\_\_\_  
Karl Runde Physics

\_\_\_\_\_  
Ray Hall Physics

For the University Graduate Committee:

\_\_\_\_\_  
Dean, Division of Graduate Studies

AUTHORIZATION FOR REPRODUCTION  
OF MASTER'S THESIS

    X     I grant permission for the reproduction of this thesis in part or in its entirety without further authorization from me, on the condition that the person or agency requesting reproduction absorbs the cost and provides proper acknowledgment of authorship.

           Permission to reproduce this thesis in part or in its entirety must be obtained from me.

Signature of thesis writer: \_\_\_\_\_

## ACKNOWLEDGMENTS

To Michelle, Katherine, and Cassandra special thanks are due for their undying love, support, and patience. I give gracious thanks to Mardell Kendall for her kindness, wisdom, and generosity during these past four years. For making both work and school scheduling possible, Steve Behm is due his rightful share of gratitude; for sure he will be grateful I am finally done!

I wish to extend my greatest gratitude to Frederick Ringwald without whose sincere desire for student achievement this work would not have been completed. Not only serving as committee chair, but acting as a mentor, Dr. Ringwald has enthusiastically challenged and encouraged me throughout my academic program. As exemplified by Dr. Ringwald, the entire Fresno State Physics Department deserves honor for their devotion, patience, and sincere concern for students.

For providing invaluable advice and insight in the development of this thesis, Brad Schaefer, Steven Saar, Karl Runde, and Ray Hall must be given due credit.

Above all, I thank our Creator for making such a fine universe in which a rich diversity of fascinating phenomena are able to be observed by humankind.

Psalm 19

## TABLE OF CONTENTS

	Page
LIST OF TABLES . . . . .	vii
LIST OF FIGURES . . . . .	viii
INTRODUCTION TO ECHOES . . . . .	1
MECHANICS OF FLARE ECHO DETECTION . . . . .	3
Categorization and History of Flares . . . . .	3
The Canonical Flare Model. . . . .	4
The Ideal Flare Profile . . . . .	11
Derivation of Echo Formulae. . . . .	12
Analysis of Formulae for the AD Leonis Example. . . . .	15
Observed Flare Characteristics. . . . .	17
Extending the Applicability of Echo Detection. . . . .	20
Signal Processing Techniques . . . . .	24
ANALYSIS OF THE METHOD. . . . .	28
Potential Problems of the Echo Detection Method. . . . .	28
Potential Benefits of the Echo Detection Method . . . . .	32
Limitations of the Echo Detection Method . . . . .	34
OBSERVATIONS . . . . .	36
Selection of Test Cases . . . . .	36
Observational Data . . . . .	41
EXPOSITION . . . . .	45
REFERENCES . . . . .	46

## LIST OF TABLES

Table	Page
1. Theoretical Planetary Semi-Major Axis as a Function of Echo Strength	21
2. Theoretical Planetary Radius as a Function of Echo Strength. . . . .	22
3. Extrapolated Counting Statistics . . . . .	23
4. Apparent Magnitudes of Hypothetical Echoes from Superflare stars.	24
5. List of Candidate Stars and Hypothetical Echo Strengths . . . . .	40
6. Information on S Fornacis and Comparison Stars Used in Time Resolved Photometry Measurements . . . . .	42
7. S Fornacis Measurement Error Statistics. . . . .	42

## LIST OF FIGURES

Figure	Page
1. Geometrical Model of an Astronomical Pulse Echo. . . . .	1
2. Elements of the Two-Ribbon Flare Model. . . . .	5
3. Electromagnetic Radiation Sources From a Flare . . . . .	7
4. Relative Energy Distribution as a Function of Time for Various Portions of Spectrum . . . . .	8
5. Light Curves of a Flare Profile from AD Leo Observed in 1984 in U- band, Ca II K, He I $\lambda$ , and H $\delta$ Emissions Lines and at 2 cm and 6 cm Radio Wavelengths. . . . .	9
6. Characteristic Profile of an Ideal Flare. . . . .	11
7. Characteristic Profile of an Ideal Flare with Echo.. . . .	12
8. Optical Flare Profile from Wolf 424 AB Observed in 1974. . . . .	18
9. U-band Observations of UV Cet Flares Recorded 18 December 1984	19
10. Comparison of Flares from EV Lac . . . . .	29
11. Distribution of Flares on Variable Star YZ CMi, Cumulative Flare Energy Verses Cumulative Flare Frequency . . . . .	31
12. Theoretical Echoes from Known Extrasolar Planets. . . . .	38
13. Photometric Data of S Fornacis (No Observed Superflares). . . . .	44

## INTRODUCTION TO ECHOES

The basic concept of flare echo detection resembles a commonplace technology dubbed radar, an acronym coined in the 1940s meaning radio detection and ranging (Harvey, 1968). The particular type of radar discussed here is a simple form of active radar where a pulse of energy is emitted from a source and the reaction of the signal to the environment is measured and analyzed by a receiver. The basic precept of active radar is that the time delay of a pulse of energy from its original source can determine the characteristics of another object.

Active radar is frequently used to determine the location, velocity, and shape of another object. A pulse of radio frequency (RF) energy is emitted from an antenna then the reflected pulse of RF energy is analyzed to determine the power and time delay of the reflected pulse or series of pulses. The analysis of the reflected pulse or pulses can provide much information about the object, provided care has been taken to filter wanted from unwanted signals (Harvey, 1968).

For most active radar systems, the originating pulse of energy is at the same location as the receiver, often using the same antenna. In the astrophysical world, which deals with large distances and very long time scales, having the transmitted signal emanate from the same physical location as the receiver is impractical. However, if the transmitted pulse were to come from a star, all that would be needed is to analyze the received pulse from Earth to determine some characteristics of the objects in the neighborhood of the star (see Figure 1).

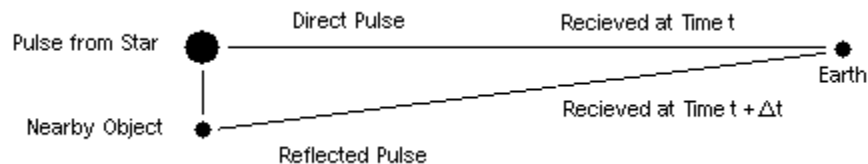


Figure 1. Geometrical Model of an Astronomical Pulse Echo

While radar uses a RF energy pulse, this method relies on a pulse of light emitted from the star. An implicit assumption is that the pulse of light propagates in all directions equally and simultaneously; that the pulse radiates isotropically. For the observer on Earth the pulse follows two paths: one directly to the observer, the other to the nearby object where the pulse is then reflected to the observer. In this model, the nearby object would be detected as a secondary pulse with amplitude decreased and at a time delay  $\Delta t$ . The amplitude reduction comes from the reflectivity and relative size of the object while the time delay is caused by the light travel time to the object. In Figure 1, the geometry has been exaggerated in order to illustrate the concept. Even for stars in the vicinity for the Solar System, the observed stars and their nearby companions are typically indistinguishable from a point source of light.

In order for radar to work properly, either the shape of the initial pulse must be predetermined, or the duration of the pulse must be short in comparison to the signal travel time in the medium to the nearby objects (Azary, 2009). For a star, the shape of the initial pulse cannot be predetermined; therefore, the pulse must be narrow in comparison to the light travel time to the nearby object. Various types of energy pulses are emitted from stars, in combinations of short and long durations with small and large amplitudes. The ideal pulse best suited for this purpose is a large amplitude stellar flare. The combination of short duration and high amplitude make the stellar flare ideal for the flare echo detection method.

## MECHANICS OF FLARE ECHO DETECTION

The variable nature of stars has a long documented history. In any portion of the sky, stars can be found in various states from quiescence to obliteration. Of the myriad of observable characteristics on either short or long timescales compared to a human lifetime, a particular type of short-term variation called flaring is here investigated.

### Categorization and History of Flares

Gershberg (2005) defines a flare qualitatively as a “fast release of a noticeable amount of energy that disturbs the steady state of the star on the whole or a part of it.” The first noted occurrence of a flare from a star other than the Sun was in 1924 by Hertzsprung. At the time of the observation, Ejnar Hertzsprung attributed the brightening of the star to an in falling asteroid. It was not until 1947 when an American astronomer, Carpenter, discovered a flare from a series of photographic exposures of a red dwarf star intended for parallax measurements. The sudden increase of intensity returned to original intensity at the end of the series. The increase in intensity was much faster than a supernova and was far less luminous. The star’s name was later changed to UV Ceti, and now most flare type stars are generally categorized by the term “UV-Cet variables.” (Henden and Kaitchuck, 1982)

Further progress in detection methods (such as photoelectric devices and later CCD detectors) led to several other types of categorizations of the variable nature of stars. For example in 1949, astronomers Gordon and Kron discovered a flare event from an eclipsing binary system now called AD Leonis (Henden and Kaitchuck, 1982). Another multi-star system BY Draconis was discovered in

1966 by Chugainov to exhibit starspots associated with the magnetic interaction of the stars (Gershberg, 2005). For modern classifications, flare stars may often be categorized as UV-Cet type or AD-Leo type depending on the source of the variability. Stars with extrasolar planets may sometimes be categorized as BY-Dra type stars. Unfortunately, the categorizations are by no means consistently applied.

There are now several sources of information on variable stars. Gershberg (1999) produced an online searchable database of *UV-Ceti type variable stars*. Sternberg Astronomical Institute in Moscow hosts the *General Catalog of Variable Stars (GCVS)* which contains many different types of variability. Whatever the categorization of variability used, of those stars known to be variable, numerous stars are known to have flares.

### The Canonical Flare Model

Over the past several decades, astrophysicists have developed many theories on the principles of flare evolution; however, the specific physics of such events have yet to be completely identified (Haisch et. al., 1991; Schrijver, 2000; Gershberg, 2005). Among a wide variety of flare models, the accepted canonical model for a class of highly energetic flares is the two-ribbon flare model. As noted by Haisch et. al. (1991), the model proposed by Martens and Kuin (1989) best provides a reference model to assist in conceptualization (see Figure 2). The two-ribbon flare model was developed out of observations of flares on the Sun.

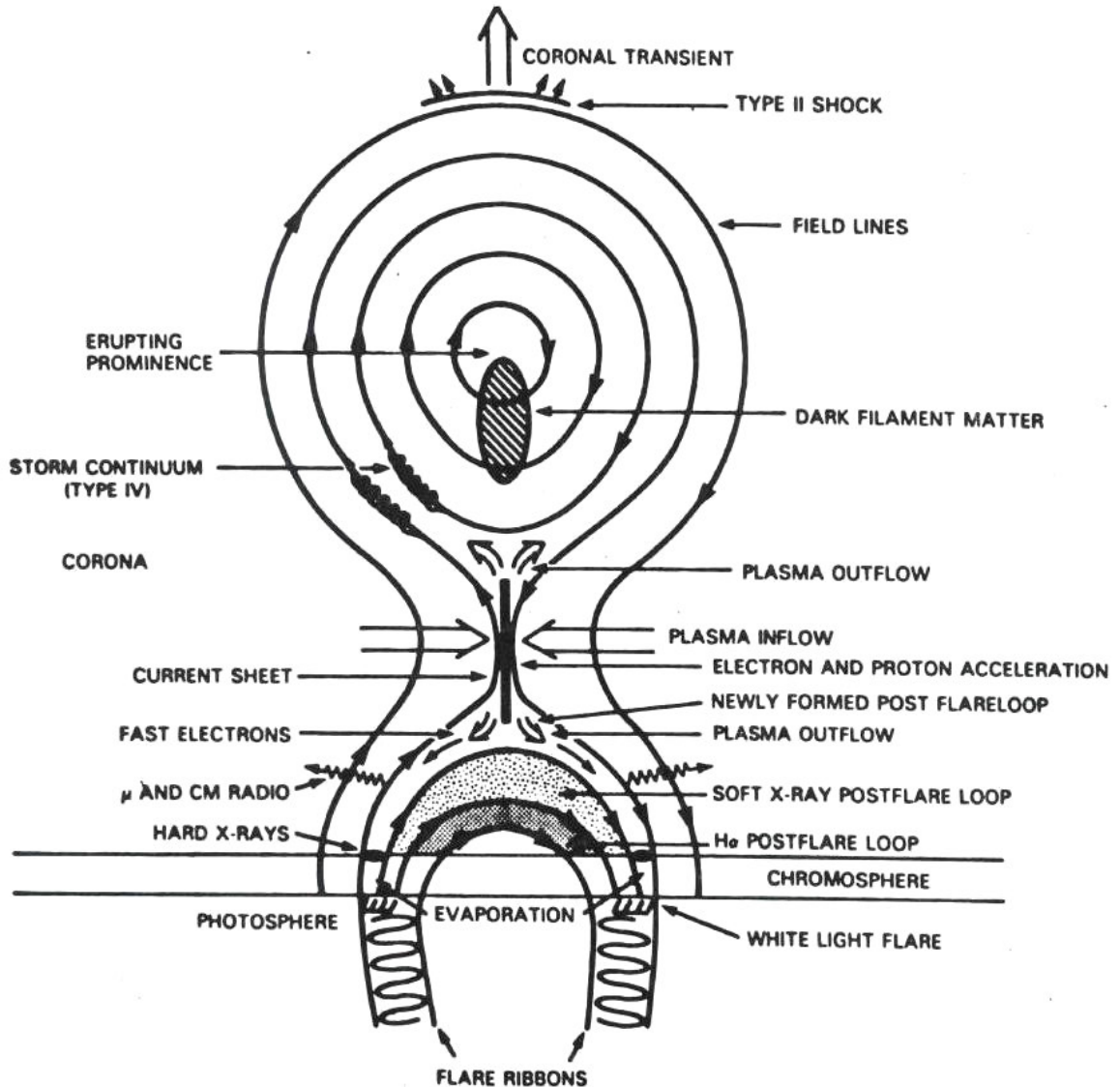


Figure 2. Elements of the Two-Ribbon Flare Model. With kind permission from Springer Science+Business Media: Solar Physics, "A Circuit Model for filament Eruptions and Two-Ribbon Flares," vol. 122, 1989, page 269, Martens and Kuin, Figure 2.

The two-ribbon flare begins with a filament, essentially a mass of cool charged particles producing a line current suspended in a magnetic field “tube” extending through the stellar atmosphere (Haisch et. al., 1991; Martens and Kuin, 1989). The connection points of the line current with the photosphere provide the endpoints of the “ribbons.” In a static (or even quasi-static) atmosphere, a balance of forces would keep the filament stationary. However all stellar atmospheres are inherently non-static (Böhm-Vitense, 1997). Prior to loss of quasi-static equilibrium, the filament may begin to twist or unravel and as so doing ascend through the atmosphere. When equilibrium is lost, the filament will erupt; the field lines of the magnetic tubes in the filament will break in much the same way as an over-twisted rubber band. Unlike a rubber band however, the field lines will reconnect. The energy released in the magnetic field reconnection provides much of the necessary energy for the two-ribbon flare. The free magnetic energy is converted into kinetic energy by particle acceleration. (Martens and Kuin, 1989; Haisch et. al., 1991)

The energy released by the accelerated particles provides chromospheric evaporation that heats the material and fills the magnetic post-flare loop with hot material. As the flare progresses, magnetic reconnection continues to produce higher arcades of loops. Once formed, the arcade of loops is disconnected from the original source of energy (originally stored in twisted magnetic fields) and the loop begins to cool. The material in the loop is then accelerated downward to the stellar surface. As the particles enter the chromosphere, a pulse of energy is released triggering a cascade of the loops. Due to the density and mass flow in the arcade structure, the lower filament tube pushes against the overlying arcade in the corona causing a Coronal Mass Ejection (CME) (Haisch et. al., 1991). During a

CME, a very large amount of energy is released in the form of charged particles and electro-magnetic radiation (see Figure 3).

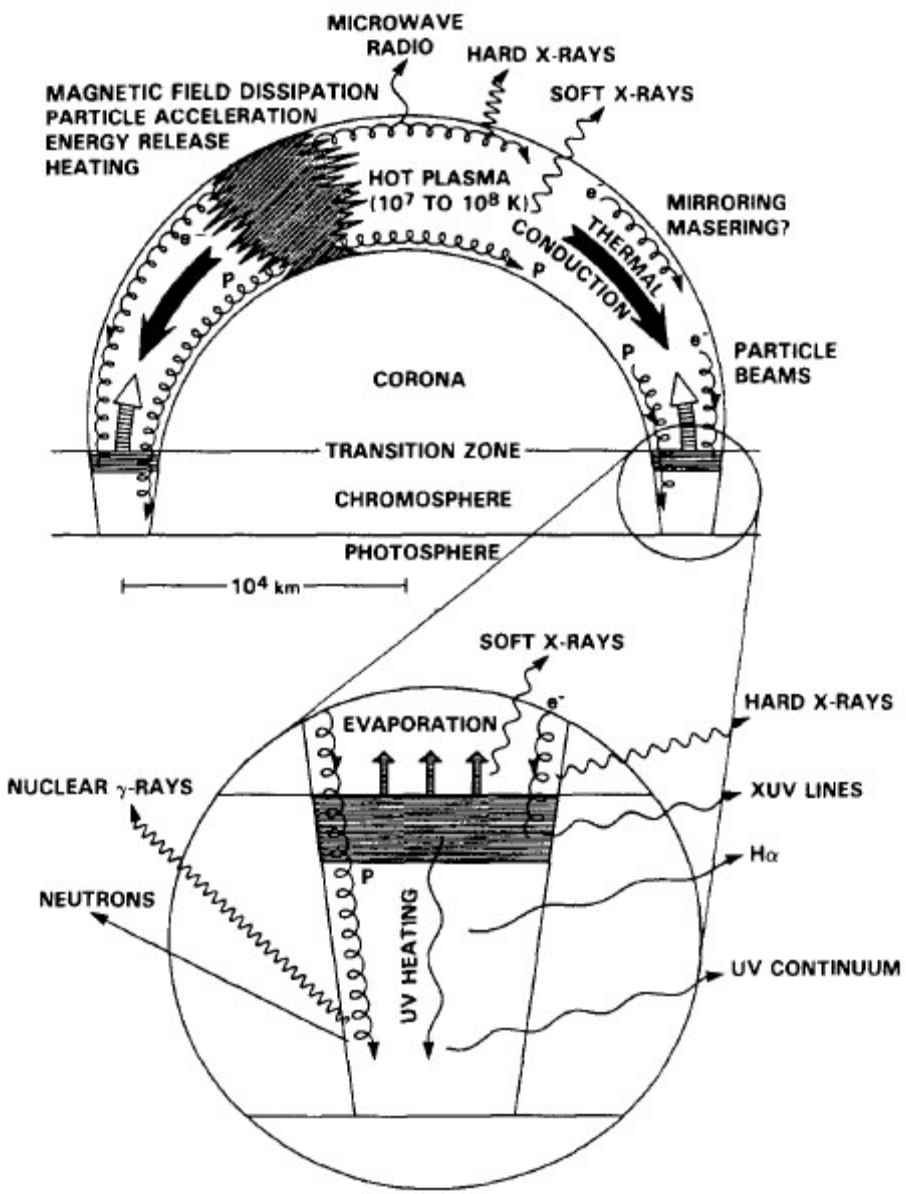


Figure 3. Electromagnetic Radiation Sources from a Flare. With kind permission from Springer Science+Business Media: Astrophysics and Space Science, "Solar Flares: The Impulsive Phase." vol. 121, 1989 page 77, Dennis and Schwartz, Figure 1.

The majority of the electro-magnetic radiation is generated in the current sheet below the filament. An impulsive white light flare is produced in the photosphere at the ribbon connection points. Soft X-rays ( $< 1$  keV) are produced at the magnetic reconnection sites from particle acceleration while hard X-rays ( $> 1$  keV) are produced in the chromosphere from the impact of fast particles returning to the stellar surface. A radio burst starts several minutes after the initial pulse. The initial pulse is visible in X-rays and UV then gradually shifts toward longer wavelengths as the loops cool. (Martens and Kuin, 1989)

The characteristics of the time profile of the flare vary depending on the wavelength of radiation observed. Additionally, the characteristics of flares exhibit very different profiles across the electro-magnetic spectrum (see Figures 4 and 5). The more energetic the flare, the more energy is placed into short wavelength spectrum.

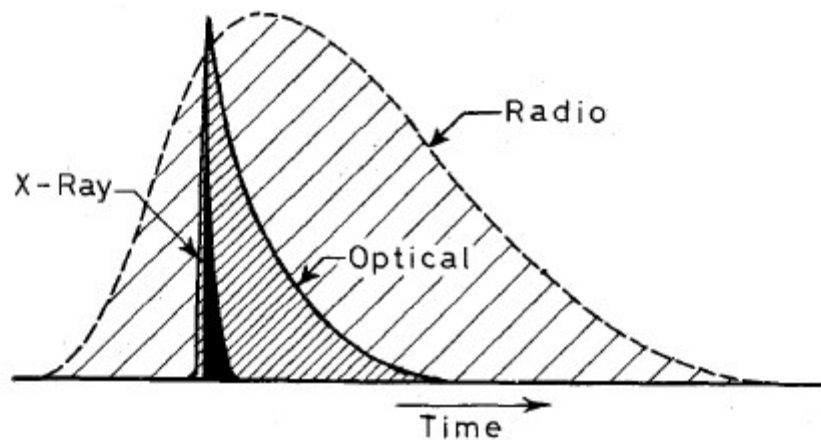


Figure 4. Relative Energy Distribution as a Function of Time for Various Portions of Spectrum. With kind permission from Springer Science+Business Media: Astrophysics and Space Science, “Flare Stars and the Fast Electron Hypothesis,” vol. 48, 1977 page 331, Gurzadyan, Figure 12.

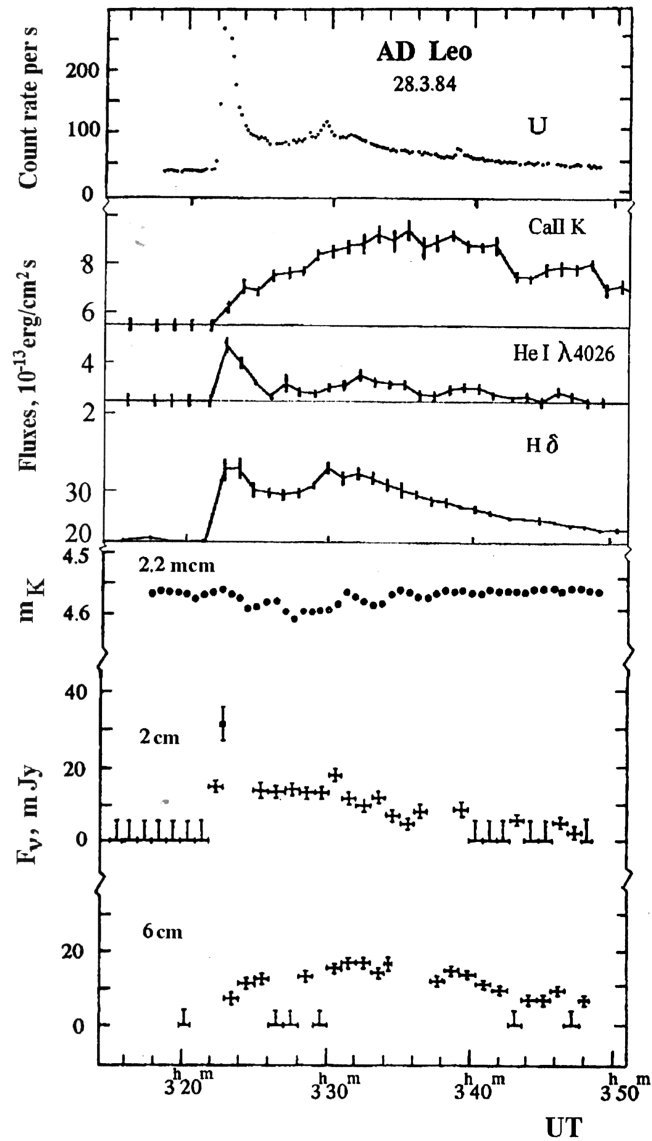


Figure 5. Light Curves of a Flare Profile from AD Leo Observed in 1984 in U-band, Ca II K, He I  $\lambda$ , and H  $\delta$  Emissions Lines and at 2 cm and 6 cm Radio Wavelengths. With kind permission from Springer: Solar-Type Activity in Main-Sequence Stars, 2005, Page 204, Gershberg, Chapter 2, Figure 29.

In order to make apposite the measurement of flares, a suitable portion of spectrum must be selected. It is undesirable to perform observations without a filter primarily due to the response of the detector used and the time delay of the flare over wavelength. The combination of effects reduces the usable time resolution from the data. Observations with no filter also tend to introduce more noise and therefore increase the echo amplitude necessary for detection (Bromley, 1992). Observations taken through a filter of narrow bandwidth increase the likelihood of detecting an echo, however decrease the number of detectable photons. It is therefore desirable to determine the best portion of spectrum for echo detection.

For high energy flares, an especially strong spike of energy is observable in the X-ray and UV spectrum. Unfortunately, for terrestrial observatories the X-ray portion of the spectrum is absorbed by Earth's atmosphere. Therefore the most likely portion of spectrum to produce the best signal to noise ratio for echo detection from terrestrial observatories is in the Ultra-Violet U-band. Depending on the telescope and the detector used, the next best alternative is the Blue or B-band. The U-band and B-band are segments of the UBVR<sup>1</sup>IJKLMN photometric system<sup>1</sup> extending through the wavelengths observable by terrestrial telescopes. The U-band is centered at 365 nm with a Full Width at Half Maximum (FWHM) of 68 nm and the B-band is centered at 440 nm with a FWHM of 98 nm (Zombeck, 1990).

The method employed for observations of flares involved measuring the intensity of the star in numerous successive finite increments (Berry and

---

<sup>1</sup> The photometric system employed here is the most commonly available. Other photometric systems offer suitable filters that may lead to equally usable results.

Burnell, 2005). This process is called time-resolved photometry. In order to make these photometric or intensity measurements, the structure of the flare profile must be understood.

### The Ideal Flare Profile

A flare is characterized by a rapid increase in the detected intensity of a star followed by a slower decrease lasting from minutes to hours. The sharp increase in energy makes flares an excellent candidate for development of the echo detection method. An idealized characteristic fast-rise-exponential-decay flare model is depicted in Figure 6. The idealized pulse of light mimics the behavior of flare profiles based on observational data (e.g. Gershberg, 2005). As depicted below, the lowest level is the ambient quiescent state of the star. In the perfect flare, the pulse would be a narrow spike of energy with the star returning to quiescent state immediately after the flare. In all flare profiles, there exists a lingering background signal; therefore, the ideal flare shown below includes a minimal contribution of background post-flare light.

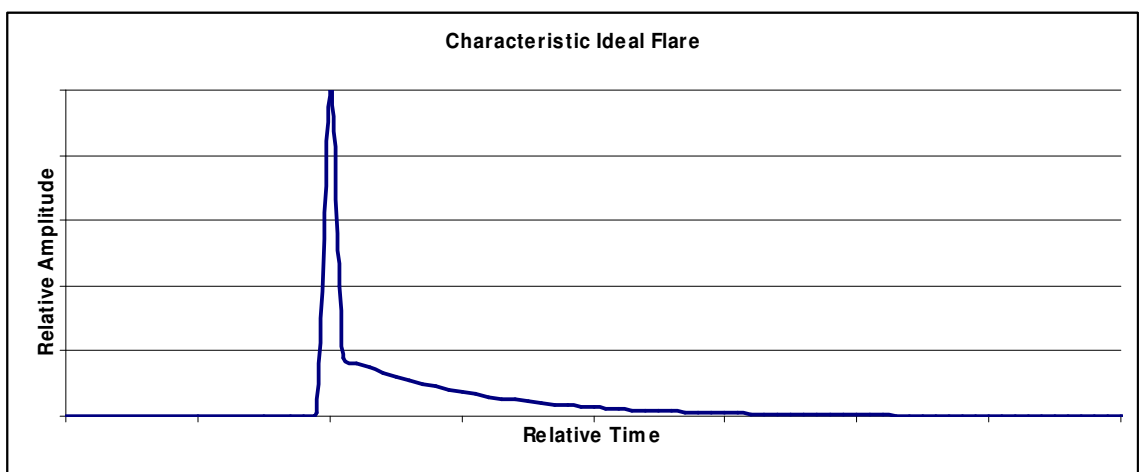


Figure 6. Characteristic Profile of an Ideal Flare

In the idealized example shown in Figure 1 on page 1, the nearby reflective object, hereafter referred to as a planet, would be detected by the observer as a secondary pulse. The detection of this secondary pulse would contain the same pulse shape as the initial pulse, however with decreased amplitude and a time delay from the initial pulse. The flare would likely resemble something approximating the profile shown in Figure 7.

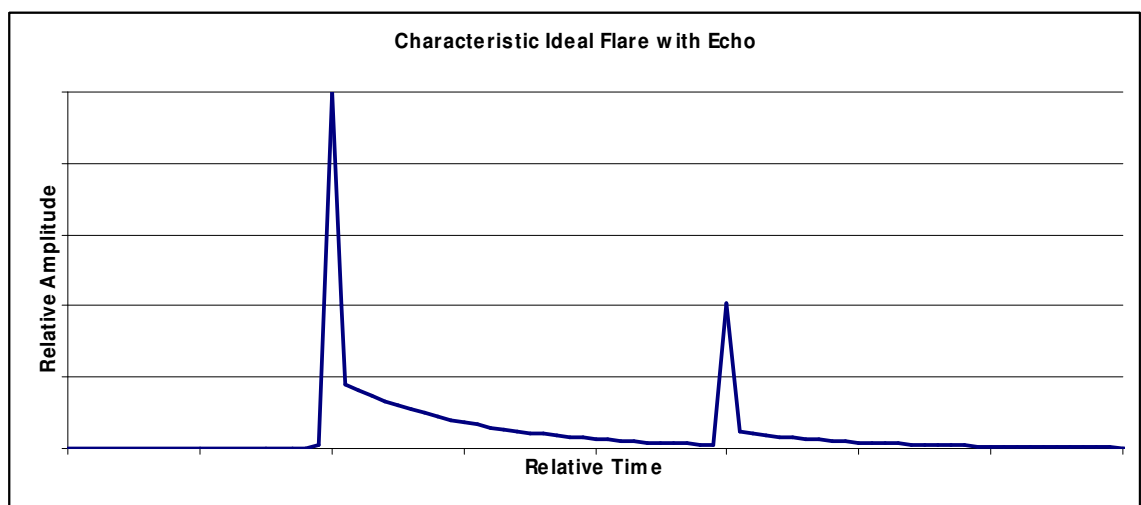


Figure 7. Characteristic Profile of an Ideal Flare with Echo

The echo from the planet gives two pieces of information, a relative change in light intensity and a relative change in time. A connection between the flare and the echo can be formulated from the flare profile using standard measurement parameters.

#### Derivation of Echo Formulae

Bromley (1992) constructed an outline for determining the existence of faint echoes in flare profiles. The method takes the measured quantities and derives a model from which information can be determined about the characteristics of the echo. The model begins with the flare signal produced at the

detector written in pure counting statistics. The total photon flux,  $L$ , in counts can be written as a linear sum of its components:

$$\text{Equation (1)} \quad L(t) = F(t) + \varepsilon \cdot F(t - \tau) + Q + N(t),$$

where  $F$  is the flare contribution,  $Q$  is the mean quiescent flux,  $N$  is the noise and the unit-less value  $\varepsilon$  (epsilon) is the echo contribution at time delay  $\tau$  (tau). Here,  $\varepsilon$  is the ratio of the intensity of the echo relative to the flare pulse. (Bromley, 1992)

Applying standard signal processing techniques, the portion of the light curve representing the flare convoluted with the light curve ( $F * L$ ) ( $t$ ) will filter out the random components of noise. To detect an echo in the profile, the weighted convoluted flare profile  $\varepsilon (F * F)(t=t_{flare})$  must be greater than the convoluted noise ( $F * N$ ) ( $t = \tau$ ). Assuming that the flare pulse duration is shorter than the light travel time to the planet, the echo occurs after the stars quiescent state has returned, and making the assumption of Poisson noise statistics for  $N$ , a lower bound for  $\varepsilon$  can be estimated. Since the detector integrates each time segment over a finite time  $\Delta t$ , the standard deviation of the signal at the quiescent state is simply  $\sqrt{Q\Delta t}$ . Therefore the minimum detectable echo strength is defined where  $\varepsilon (F * F)(t=t_{flare})$  is equal to ( $F * N$ ) ( $t = \tau$ ),

$$\text{Equation (2)} \quad \varepsilon_o F_{max} \Delta t \approx \sqrt{Q\Delta t},$$

where  $F_{max}$  is the flare amplitude at maximum light (assumed constant over  $\Delta t$ ) (Bromley, 1992).

For convenience, a parameter  $f$  is defined such that  $f = F_{max} / Q$ . Now the minimum detectable echo strength can be rewritten as,

$$\text{Equation (3)}^2 \quad \varepsilon_0 \approx \frac{1}{F_{max}} \sqrt{\frac{Q}{\Delta t}} = \frac{1}{f} \sqrt{\frac{1}{Q\Delta t}}.$$

---

<sup>2</sup> The original paper incorrectly displays Equation 3 with  $\Delta t$  in the numerator.

Also for convenience, another parameter  $a_0$  can be defined which characterizes the detection limit,

$$\text{Equation (4)} \quad a_0(f) = \frac{1}{f\sqrt{Q_s}},$$

where  $Q_s$  is the flux of photons at the quiescent stellar surface. As Bromley (1992) points out, the advantage to  $a_0$  is that the parameter depends only on intrinsic properties of the star, the effective temperature during the quiescent state, and the flare amplitude.

By assuming a geometrical approach as in Figure 1 on page 1 for a compact spherical object, the echo strength is scaled by the reflectivity of the planet, the relative size or radius of the planet, and the planet's distance from the host star. This geometrical approach sets the upper limit for an echo detection since it does not take into account any detection parameters,

$$\text{Equation (5)} \quad \varepsilon = A \cdot \left(\frac{r}{d}\right)^2,$$

where  $r$  is the planet radius,  $d$  is the distance of the planet from the host star and  $A$  is the object's albedo. Comins and Kaufmann (2005) define the term "albedo" as the fraction of incident light returning directly to space.

Putting together other systematic parameters, such as telescope aperture, detection limits due to noise and detector efficiency the expected lower echo strength limit for a given telescope configuration can be derived,

$$\text{Equation (6)} \quad \varepsilon \geq a_0 \frac{D}{R} \frac{1}{\sqrt{ac\Delta t}}. \quad (\text{Bromley, 1992})$$

Rewriting Equation 6 without substitutions, the form of the lower limit can be expressed as,

$$\text{Equation (7)} \quad \varepsilon \geq \frac{Q \cdot d}{F_{\max} \cdot r \cdot \sqrt{Q_s ac\Delta t}},$$

where for both Equations 6 and 7 with all other terms being previously defined,  $a$  is the collecting area of the detector and  $c$  is the quantum efficiency of the detector.

Analysis of Formulae for the AD Leonis Example:

To better understand the detection method, the example of AD Leonis given by Bromley (1992) is re-analyzed. For the purpose of exploring the equations, the detection limit parameter defined by Equation 4 is not employed however in practical application this parameter would prove useful.

The formulae use purely counting statistics as one would measure using a CCD detector. Bromley assumes a U-band filter for reasons discussed previously. In order to avoid confusion by syntax, the following terms are defined:

$R_{\text{sol}}$  = Radius of the Sun

$R_{\text{jup}}$  = Radius of Jupiter

$R_*$  = Radius of the star

$L_{\text{sol}}$  = Luminosity of the Sun

$L_*$  = Luminosity of the star

$T_{\text{eff}}$  = Effective Temperature

For the test case of AD Leonis, a M4.5V star, the follow parameters are assumed: the apparent magnitude in U-band ( $^m\text{U}$ ) is 12.2, the effective temperature of the star ( $T_{\text{eff}}$ ) is 2950 K (nearly equivalently  $L/L_{\text{sol}}=0.04$ ) which is based on the M4.5V classification of the star, the measured parallax ( $p$ ) is 213 milli-arcseconds ( $mas$ ) (SIMBAD, 2008), the ratio of the radius of the star to the radius of the sun ( $R_*/R_{\text{sol}}$ ) is 0.4, and that the given flare magnitude  $\Delta^m\text{U} = 4.0$ .

In terms of the equipment setup, we assume the same example used in the original analysis (Bromley, 1992), that a 1 m telescope is used, the detector area is

approximately  $6.5 \text{ cm}^2$ , the quantum efficiency of the detector  $c$  is 0.25, and the detector integration time,  $\Delta t$  is 10 s.

Translating the input parameters into counts requires some conversions. Starting with the quiescent magnitude of the star, we can derive the flare magnitude by,

$$\text{Equation (8)} \quad m_{\text{flare}} = 12.2 - 2.5 * \text{LOG}(1 + 10^{0.4 * \Delta U}).$$

Therefore, the apparent flare magnitude is 8.17. The value for  $F_{\text{max}}$  can be obtained from inverting the definition of the magnitude standard in the U-band where  $I_u$  is the flux and  $F$  takes into account the detector used,

$$\text{Equation (9)} \quad I_u (\text{ergs/cm}^2/\text{\AA}/\text{s}) = 4.27 \times 10^{-9} * 10^{\frac{m_U}{-2.5}} \quad (\text{Zombeck, 1990})$$

$$\text{Equation (10)} \quad F_u (\text{counts/s}) = \left(\frac{d}{2}\right)^2 \cdot \frac{I_u \cdot \pi \cdot c \cdot \lambda_{\text{eff}} \cdot \Delta \lambda}{h \cdot c'}$$

where  $d$  is the linear aperture (diameter) of the telescope,  $\lambda_{\text{eff}}$  is the effective center of the photometric band,  $\Delta \lambda$  is the integration width of the photometric filter,  $c$  is the quantum efficiency of the detector (with an assumed value of 0.25),  $c'$  is the speed of light,  $h$  is Plank's constant.

For the maximum flare amplitude, Equation 9 shows the maximum flare flux,  $I_{u-\text{max}} = 2.24 \times 10^{-12}$  (ergs/cm<sup>2</sup>/\AA/s) and from Equation 10,  $F_{\text{max}} = 5400$  counts per second. For the quiescent state of the star, again using Equations 9 and 10,  $Q$  is determined to be 132 counts per second.

The distance to AD Leonis is determined from the measured parallax,

$$\text{Equation (11)} \quad D (\text{cm}) = 3.08 \times 10^{21} / p_{\text{mas}},$$

so  $D = 1.45 \times 10^{19}$  cm. The radius of the star is determined from that of the Sun,

$$\text{Equation (12)} \quad R_* = (R_*/R_{\text{sol}} - \text{ratio}) * 6.69 \times 10^{10} \text{ cm},$$

therefore  $R_* = 2.78 \times 10^{10}$  cm.

The mean quiescent flux as the surface of the star is derived assuming a spherical power density function from the sun and scaling that with the effective temperature of the star using the Stephan-Boltzmann law,

$$\text{Equation (13) } F_* = F_{sol}(T_*/T_{sol})^4.$$

Using Equations 9 and 13, the stellar flux can be derived using the known solar flux in quiescence,  $I_* = 1.7 \times 10^{10}$  (ergs/cm<sup>2</sup>/s) or equivalently a flux of  $6.2 \times 10^{22}$  counts per second over all wavelengths. When flux is converted corrected for just the U-band this value is reduced to  $9.46 \times 10^{19}$  counts per second.

For the present example, the minimum detectable echo strength is calculated using the U-band filter by substituting the parameters calculated above into Equation 3. This sets the value of  $\epsilon_0$  at  $7 \times 10^{-4}$  and using Equation 6, calculating the echo strength limit sets  $\epsilon$  at  $9 \times 10^{-6}$ . If the telescope configuration was changed for a 4-meter telescope then the value of  $\epsilon$  becomes  $6 \times 10^{-7}$ .

This does lend validity to the calculated values since for a larger telescope; the detection of lower echo strength would be expected. This test case also shows that given a highly energetic flare, an echo from the flare is likely to be detected; this echo is not below the detectability threshold for the test case presented. Nevertheless, this does lead to the question of whether the flare characteristics used for the test case are valid for other stars.

### Observed Flare Characteristics

Although flare profiles generally exhibit certain characteristics, such as a sharp rise in intensity, the specific structure of individual flares may vary significantly. The profiles observed from consecutive flares from the same star do not show consistency in the time domain (Gershberg, 2005; Haisch et. al., 1991). Additionally, time between reoccurrences and flare energies typically follow a

nearly Poisson distribution (Gershberg, 2005). As a consequence of the chaotic behavior, the canonical model of flares does not adequately address the variety of different phenomena observed (Haisch et. al., 1991).

The characteristic fast-rise, exponential decay is still present as depicted in the ideal model (Figure 6, page 19), however observed flare profiles may exhibit other features such as depicted in Figures 8 and 9.

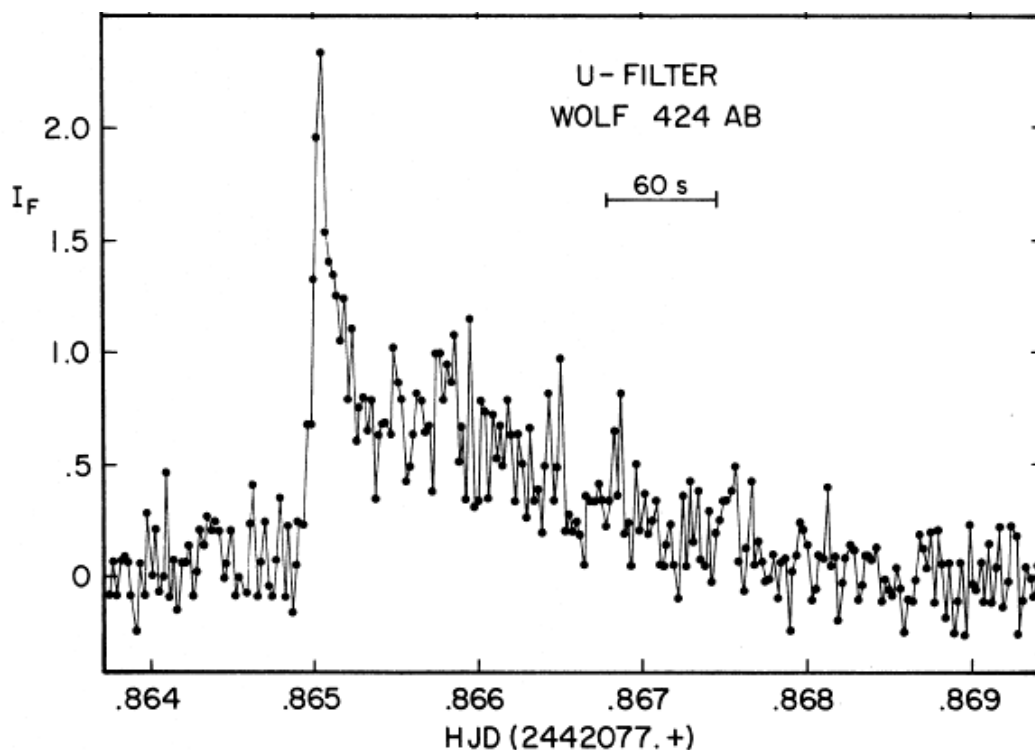


Figure 8. Optical Flare Profile from Wolf 424 AB Observed in 1974. With kind permission from Springer: Solar-Type Activity in Main-Sequence Stars, 2005, Page 200, Gershberg, Chapter 2, Figure 26, Adapted.

In Figure 8 above, the post flare characteristic flickering and background noise are shown in the flare profile. In Figure 9 below, the characteristic sympathetic flare and random nature of flare profiles are shown.

## UV Cet

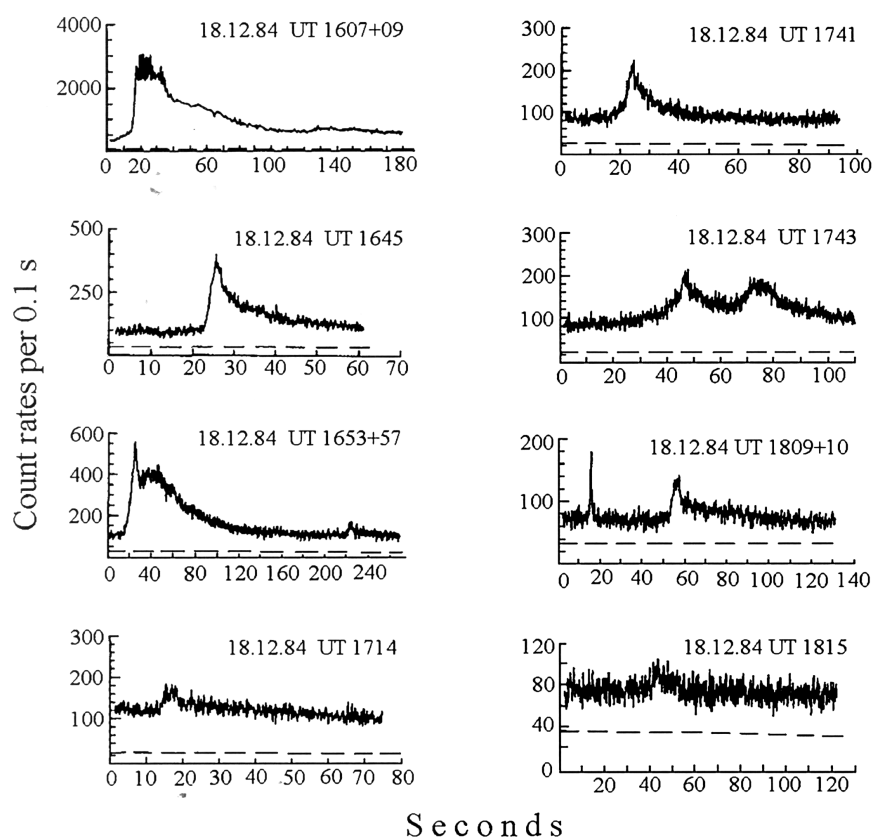


Figure 9. U-band Observations of UV Cet Flares Recorded on 18 December 1984. With kind permission from Springer: *Solar-Type Activity in Main-Sequence Stars*, 2005, Page 195, Gershberg, Chapter 2, Figure 21.

### Extending the applicability of echo detection

In the local singular example of the Sun, there is (comparatively) quite little flare activity as one might expect for an average low-mass star with a moderate magnetic field (Byrne and Rodonò, 1982; Rubenstein, 2001; Gershberg, 2005). Contrary to the expected lack of variability, Brad Schaefer (2000) and Eric Rubenstein (2001) compiled a list of stars similar to the Sun that have shown some very energetic flares dubbed “superflares”.

In the search for an explanation, Rubenstein (2001) turned to the example of close binary companion stars that exhibit flare activity due to the interaction of the magnetic fields of the two stars. Similarly for planets, the magnetic field lines of the star - planet system are interwoven which can induce higher levels of magnetic activity than would otherwise be present in the star alone (Shkolnik, et. al, 2005; Cranmer and Saar, 2007; Lanza, 2008). The question initially posed by Rubenstein (2000) suggested that magnetized extrasolar planets are a possible cause of flares from solar-type stars. Rubenstein inferred that there must be a mechanism to create such a release of energy when there is expected to be little activity.

Kashyap, et. al. (2008), have determined that there is indeed an observable byproduct of star – planet interaction. For planets close to their parent stars, the interaction comes in two forms: tidal and magnetic. Under tidal interactions,

$$\text{Equation (14)} \quad h \propto \frac{M_p R_*^4}{M_* d^3},$$

where  $h$  is the height of the tidal bulge,  $M_p$  and  $M_*$  are the mass of the planet and star respectively,  $R_*$  is the radius of the star, and  $d$  is the distance of the planet from the host star. For the magnetic interaction, the energy released during a

reconnection event for a star's stellar wind interacting with a planet's magnetosphere,

$$\text{Equation (15)} \quad F \propto \frac{B_p B_* \cdot v_{rel}}{d^n} \Big|_{n=2, far}^{n=3, close},$$

where  $F$  is the flux due to the interaction,  $B_p$  and  $B_*$  are the magnetic fields of the planet and star respectively,  $v_{rel}$  is the relative velocity between the magnetic stellar wind and the planet's magnetosphere, and  $n$  is 3 for close planets and 2 for planets far from the star.

At the time of original writing, Bromley (1992) accurately addressed the known extrasolar planet characteristics, however unknown at that time were even more extreme cases; where large planets were found close to their parent stars. As is now known, at least 30% of stars have planets (Gershberg, 2005) which were unknown when Bromley's paper was published. In order to determine what promise echo detection has, the list of planets known as of January 1, 2009 was investigated.

Assuming a static planet size (1 Jupiter radius) with the albedo set at an assumed value of 0.5 and a 1-magnitude flare, the theoretical value of  $\epsilon$  is varied. Equation 5 is solved for the orbital radius ( $d$ ) to determine at what distance such an echo is expected to be detected (see Table 1).

Table 1. Theoretical Planetary Semi-Major Axis as a Function of Echo Strength

$\epsilon$	$1 \times 10^{-7}$	$1 \times 10^{-6}$	$1 \times 10^{-5}$	$1 \times 10^{-4}$
$D_{\text{planet}}(\text{AU})$	1.07	0.34	0.11	0.034
$P_{\text{orbit}}(\text{Days})$	402	72.4	13.3	2.290

For reference, Table 1 includes the calculated orbital period according to Kepler's third law. For echo strengths above  $10^{-4}$ , the theoretical planetary semi-major axis decreases below the present lower limit for the orbital period of known

extrasolar planets of 1.2 days (Transitsearch, 2009) which indicates an upper limit for the echo strength in the test case.

Taking the opposite approach, a semi-major axis of 0.05 AU is assumed, which is consistent with the “Hot Jupiter” model. Varying the theoretical value of  $\epsilon$ , Equation 5 is solved for the planet radius. Assuming a 1-magnitude flare with the albedo set at an assumed value of 0.5, Equation 5 is solved for the planet radius. At  $\epsilon = 1 \times 10^{-4}$ , the theoretical planet radius is 1.5 times that of Jupiter.

Table 2. Theoretical Planetary Radius as a Function of Echo Strength

$\epsilon$	$1 \times 10^{-7}$	$1 \times 10^{-6}$	$1 \times 10^{-5}$	$1 \times 10^{-4}$
$R_{\text{planet}}(R_{\text{jup}})$	0.05	0.15	0.47	1.48

In this example, the planetary radius reaches an unphysical maximum. The largest radius for a planet is approximately that of Jupiter. Due to gravitational self-energy, a body with more mass than Jupiter will exhibit electron degeneracy and thus remain at a near constant radius as a function of mass up to and including the mass of a brown dwarf (Comins and Kaufmann, 2005). Tables 1 and 2 together give an indication of the limits of echo detection for the indicated parameters. From the geometrical calculation in combination with a 1-magnitude flare with echo strength of  $10^{-5}$ , it is likely that an echo would be near the limits of detection for a small terrestrial observatory.

While the geometrical echo model provides insight to the upper limit for echo detection, the actual response of the detector must also be considered. In order to explore the photon counting statistics,  $F_{\text{max}}$  is assumed at 10000 counts per second while the echo strength is varied. To determine total counts, integration times have been chosen such that there are at least 10 counts per exposure. Exploration of the anticipated measurements shows the expected counts

extrapolated for a flare of fixed amplitude with varying echo strength,  $\epsilon$ . This exercise shows that the dominating noise source for such measurements is likely to be scintillation noise due to atmospheric effects and shot noise due to lack of photons.

Table 3. Extrapolated Counting Statistics

$\epsilon$	$1 \times 10^{-7}$	$1 \times 10^{-6}$	$1 \times 10^{-5}$	$1 \times 10^{-4}$
$F_{\text{echo}}$ (cps)	0.001	0.01	0.1	1
$\Delta t$ (sec)	10000	1000	100	10
Total counts	10	10	10	10

In further attempt to quantify the expected observable characteristics of flares and flare echoes, the list of superflare stars from Schaefer (2000) and Rubenstein (2001) was used to calculate the expected apparent magnitudes of the flare echo. The calculation assumes that a planet exists orbiting each star with a 1-Jupiter radius, an orbital semi-major axis of 0.05AU, and an albedo of 0.5. Since the U-band quiescent apparent magnitudes were not readily available, the B-band apparent magnitudes are used (SIMBAD, 2008). A further assumption has been taken that the flare energy listed for each flare star from Schaefer (2000) and Rubenstein (2001) is contained entirely in the B-band; this will tend to overestimate the apparent magnitudes.

The calculations compare the flare magnitudes to that of the known total B-band flux of the Sun. The B-band stellar flux is then compared to the known solar B-band flux. Then the absolute magnitudes are calculated knowing the parallax of the star. The flux from the flare and echo are calculated at the surface of the star, rewritten into absolute magnitudes and then corrected back to apparent magnitude. Since the echo flare strength has been set by Equation 5 the delta

magnitude from flare to echo is fixed at  $\Delta^m B = 10.85$ . Table 4 illustrates that the observed parameters of the echo are quite faint.

Table 4. Apparent Magnitudes of Hypothetical Echoes from Superflare Stars.

Star Name	$^m B_{\text{echo}}$
Groombridge 1830	19
Kappa Ceti	21
Pi1 Ursae Majoris	25
S Fornacis	19
BD + 10°2783	27
Omicron Aquilae	20
5 Serpentis	21
UU Corona Borealis	23
i Cet	26

### Signal Processing Techniques

To obtain the flare profile, the standard method of time-resolved differential photometry is employed. In direct photometric analysis, the photometry for each star to be measured is performed by drawing a circle around the central maximum called an aperture, and by drawing a sky ring between a defined inner radius (greater than the aperture radius) and an outer radius. For the variable star (V), the total pixel value inside the aperture is subtracted from the total pixel value measured in the sky ring thus minimizing the effects of atmospheric turbulence.

Non-variable check stars are used for comparison with the variable star measurements. A minimum of two check stars are used (C1 and C2). To obtain the differential photometry, the photometric data from C1 is differenced from V ( $V-C1$ ). This gives the characteristics of the variations observed from the variable star. The same is performed for C1 and C2 ( $C1-C2$ ) which gives the characteristics of system noise levels. When more than two check stars are used, a third parameter may be calculated from the difference of V and the Ensemble of

check stars ( $V_{ens}$ ). The ensemble data is calculated as a root sum squares of the individual check stars and is intended to reduce the error bars of the measurement (Berry and Burnell, 2005).

As an alternative to the direct approach using aperture time resolved photometry, Sugerman (2003) suggests Point Spread Function (PSF) matched difference imaging as a viable solution to detecting faint echoes in stellar light curves. The PSF-matched images are subtracted to remove all sources of constant flux leaving only the variable sources. Sugerman (2003) argues that direct photometry does well to remove resolved point sources, however has difficulty identifying faint surface brightness features with the fluctuations of an unresolved background. The difference of two PSF-matched images will remove the unresolved sources leaving only the background statistical noise. Although the signal to noise ratio increases by a factor of  $\sqrt{2}$ , the signal to noise ratio necessary for a statistically significant measurement needs only be 2 to 3 per pixel in order for the echo to appear unambiguously above the background.

Whether photometry or PSF-matching is used, the data output produces a flare profile in a series of discrete quantities extending over a finite interval. In the analysis of flare echoes, the flare profile was convoluted with the light curve to minimize noise ( $F * L$ )( $t$ ) (Bromley, 1992). This leads to a direct application of digital signal processing using Finite Impulse Response (FIR) filters commonly employed in a variety of applications from audio processing to radar signal analysis.

A FIR filter is one type of Linear Time-Invariant filters having the advantage of both time and frequency domain analysis. The linear nature of the filter avoids problems such as harmonic and inter-harmonic distortion produced in non-linear filters (Smith, 2009). Windowing is one implementation of FIR

filtering where a “window” of some finite length is filtered with the input signal. The outcome of the filtering depends on the contents of the “window”. The filter is processed according to the FIR transfer function, a z-transform of the impulse response,

$$\text{Equation (16)} \quad H(z) \triangleq \sum_{n=-\infty}^{\infty} h_n z^{-n} = \sum_{n=0}^M b_n z^{-n},$$

therefore the transfer function of every length  $N=M+1$  FIR filter is an  $M^{\text{th}}$  - order polynomial in  $1/z$  (Smith, 2009).

In a personal interview with Zoltan Azary, a staff scientist working for Agilent Technologies, the use of FIR filtering was first suggested. Using a capable DSP tool, an appropriately sized time slice of the initial flare profile can be used in the filter. The flare sample would be time reversed and applied through the FIR filter to the original light curve. The output of the filter would produce a correlation curve in which possible “matches” to the original flare would be represented as peaks. The maximum peak would correspond to the flare itself, and an echo would be represented by a smaller peak at time delay  $\tau$  from the central peak. (Azary, 2009)

In the correlation curve, other peaks will appear near the central peak due to the nature of the filter. Flare echoes with time delay near the resolution limit, set by the light travel time to the planet, will be much more difficult to detect (Azary, 2009). In classical radar signal analysis where the signals are emitted and received at the same location, the range to the object is:

$$\text{Equation (17)} \quad R = \frac{c' \Delta t}{2} \quad (\text{Harvey, 1968; Dorf, 1993}),$$

where  $R$  is the distance of the object to the signal source,  $\Delta t$  is the time between the original pulse and the echo, and  $c'$  is the speed of light. This assumes Euclidean geometry and that the pulse emitter and the receiver are at the same

physical location. However, since in this method the pulse is transmitted near the object under investigation, the range to the planet can be approximated by,

$$\text{Equation (18) } R = c' \Delta t .$$

The resolution limit for the pulse duration of the flare is therefore set by Equation 18. For a nearby planet with an orbital semi-major axis of 0.05 AU, the maximum pulse duration for the resolution limit is 25 seconds. As noted above, the actual resolution limit may be somewhat smaller due to the time side lobes in the correlation curve.

## ANALYSIS OF THE METHOD

As with all extrasolar planet detection methods currently in use, there are some problems, benefits, and limitations with this method.

### Potential Problems of the Echo Detection Method

While flares in general can produce a pulse of energy useful for echo detection, the use of flares presents several problems stemming primarily from a lack of repeatability in the observational data. One such problem is that flares suffer from the “snowflake” syndrome: no two flares are alike (Byrne, 1983; Gershberg, 2005; Haisch et. al.,1991). In Figure 10, the flare profiles of several flares from flare star EV Lac are recorded. Although the flares are all from the same star, the characteristics of each flare are notably different. The unpredictable nature of the light curve makes observations of flare echoes difficult to experimentally verify with repeated measurements. An additional complication is the assumption that the flare events occur singularly. As observed in Figure 10, flares may occur with secondary effects such as flickering, sympathetic flaring or multi-flare events.

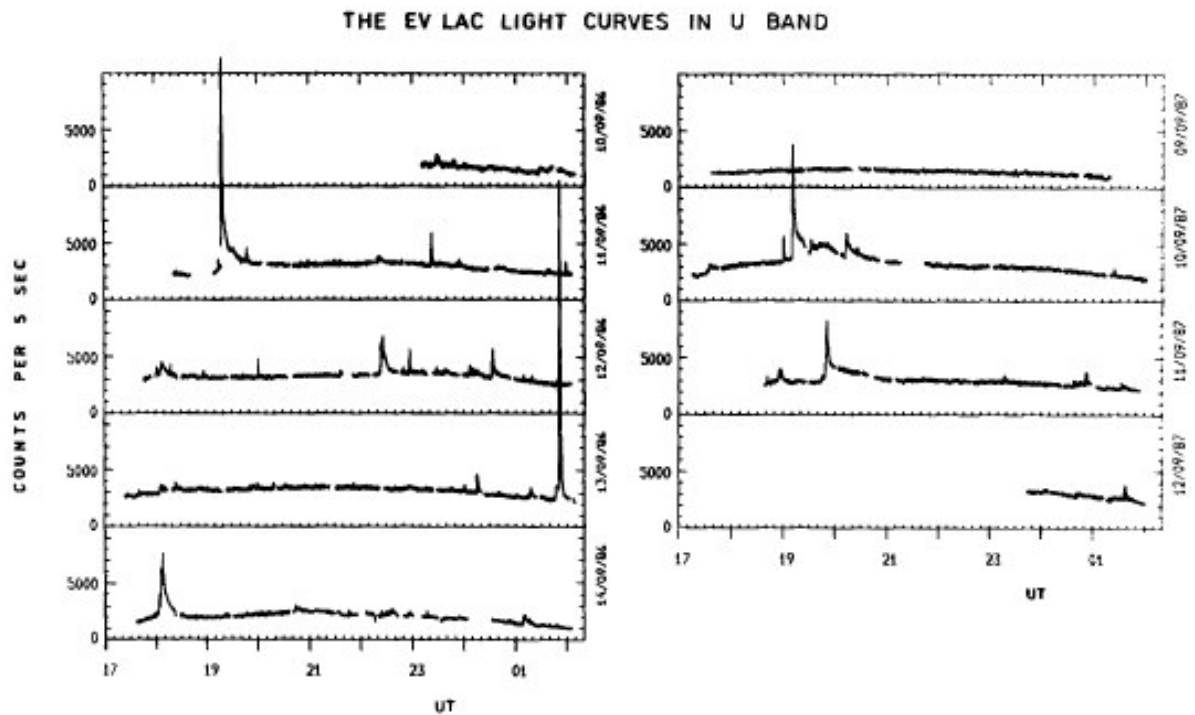


Figure 10. Comparison of Flares from EV Lac. With kind permission from Springer Science+Business Media: Solar Physics, “Stellar Flare Statistics – Physical Consequences”, vol. 121, 1989, page 376, Shakhovskaya, Figure 1.

Another form of a stellar flare’s random behavior is that of flare timing. Since flares recur with unpredictable regularity, it is difficult to determine the best time for observations of the star. This is analogous to a problem experienced by early extrasolar planet searches: the search must extend for a long period likely finding nothing at all until at last a timely observation is made. Also analogous to all methods is the likelihood of missing the signal altogether simply due to a missed opportunity window. In order for an echo to be detected, the planet must be in such a configuration as to have some portion of the illuminated disk facing the observer. Therefore, like other methods, some level of serendipity is expected.

Although flares have been observed to occur, there exist still scant data regarding the frequency of occurrence of energetic short duration flares. Indeed,

like terrestrial weather, the very nature of the phenomena demands unpredictability due to the non-linear nature of the system. Consequently, the time between superflares may be longer than a human lifetime for some stars. It is also noted by Shkolnik, et. al.(2008), the cyclic variations in star-planet magnetic interactions produce a cycle of magnetic activity. For the echo detection method, this means that there may be cyclic variations in the flare activity creating periods of immense activity and periods of little or no activity (Shkolnik, et. al. 2004). The combination of the unpredictable nature of flares and the cyclic on/off periods of activity produces the potential to consume vast amounts of telescope time with a high risk of obtaining no useful data (Schaefer, 2009).

Observational data from other stars not known to harbor nearby giant planets indicates an inverse relationship between the number of flares and the energy of the flare (see Figure 11). This indicates low-energy flares tend to occur more frequently while high-energy flares tend to occur less frequently. Dimitrov and Panov (2004) provide the line fit to the data given in Figure 11 in the following relationship,

$$\text{Equation (19) } \text{Log}(\nu) = 22.1 - 0.73 \cdot \text{Log}(E_u),$$

where  $\nu$  is the cumulative flare frequency  $\nu = N/T$  and  $E_u$  is the flare energy in the U-band. As also indicated in Figure 11, Schaefer (2009) notes in a personal communication that the superflares necessary for successful echo detection are likely to be rare. This creates a significant obstacle to advance planning for observations of flare stars.

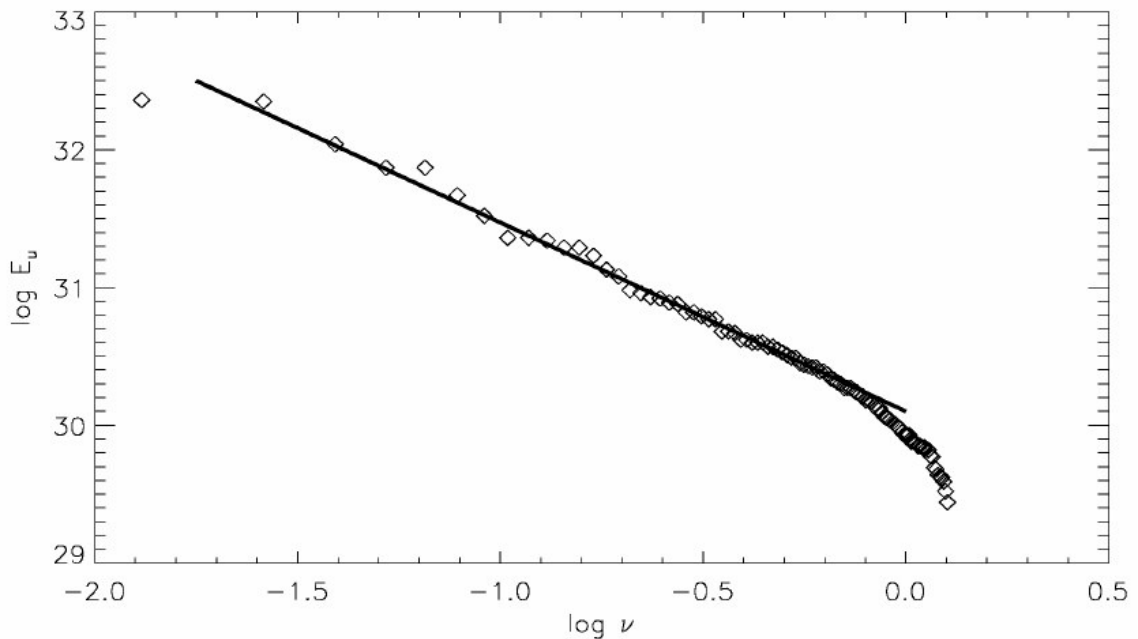


Figure 11. Distribution of Flares on Variable Star YZ CMi, Cumulative Flare Energy Verses Cumulative Flare Frequency. (Dimitrov and Panov, 2006).

For those rare times when a superflare may occur, there is an observed background phenomena. During spectroscopic observations of energetic flares, the Ca II H and K lines are known to remain visible long after the initial flare pulse (Gershberg 2005). The Ca II H and K lines are indicators of chromospheric activity. This means that the star's upper atmosphere is being churned during and after a flare event. There are some indications that the presence of a planet enhances Ca II H and K emissions (Cranmer and Saar, 2007) which demonstrates that a planet's magnetic field does interact with the magnetic field of its host star. While the Ca II H and K emissions can be removed through spectral filtering, the chromosphere of the star may have emissions in other bands which otherwise may not have been present within the passband of the filter. The consequence as it applies to echo detection is a lingering chaotic background signal problem in certain portions of the spectrum as noted in Figure 8 on page 26

previously. This lingering and unpredictable signal may likely resemble the flare profile and produce false detections in the correlation curve.

The theoretical model presented assumes the planetary albedo to be approximately 0.5. This assumption is valid for Jupiter-type planets since the albedo of Jupiter is 0.52 (Comins and Kaufmann, 2005). However, the atmospheric characteristics of the “Hot Jupiter” model may be significantly dissimilar from the classical Jupiter model. Rowe et. al. (2008) estimated the upper limit of the albedo on giant extrasolar planet HD 209458b as 0.12. This datum indicates that for a planet with a known orbital semi-major axis of 0.047 AU, the atmospheric conditions for cloud formation are differ from the classical Jupiter model. It is proposed that due to the planet’s proximity to the parent star the increased surface temperature is well suited to producing a molecular haze that absorbs incident UV photons however the underlying atmospheric physics is not well-understood (Rowe et. al., 2008).

#### Potential Benefits of the Echo Detection Method

There are several benefits to flare echo detection, largely because the method is vastly different from either radial velocity or planetary transit methods. Like the planet transit method, flare echo detection also has the potential for discovering characteristics of the planet’s atmosphere when used in conjunction with high-resolution spectroscopy. Although direct measurements of the planet’s atmosphere are unlikely, an indication of the atmosphere’s response to incident light will be displayed in the scattered light in the echo.

The measurement of the echo’s time delay and relative amplitude will directly measure the coupled albedo, orbital inclination, and planet radius. This information is readily obtainable during extrasolar planet transits; however, this is

likely only 1 to 3% of the extrasolar planet population. Information on the radius of extrasolar planets is simply unattainable from radial velocity surveys.

Therefore, the information contained in the echo would give a parameterization, which if performed in conjunction with spectroscopy may lead to the identification of the bounded limits for the coupled parameters.

Unlike radial velocity measurements and transits, this measurement technique is less sensitive to the orbital inclination of the system. Obviously, there is some geometrical advantage to having the orbital inclination near edge-on, since this provides the highest reflectivity in the direction of the observer. Nevertheless, in comparison with other methods, the required inclination limits are relaxed.

Another benefit of the method is contained within the flare phenomena itself; as pointed out by recent research there exists a correlation with close-in planets and increased stellar activity (Kashyap, et al., 2008; Lanza, 2008; Shkolnik, 2008; Lanza, 2009). Approximately 30% (Kashyap, et. al., 2008) of the stars harboring known extrasolar planets shown increased X-Ray activity indicating increased rates of magnetic reconnection events as the magnetic fields of the star and planet interact. The increased X-Ray activity does not necessarily imply the occurrence of flares; however, in such environments, flares are more likely to occur.

Although the on/off nature of the magnetic interactions was listed as a problem, it can also be used as a potential benefit. Since the magnetic activity can be monitored in the Ca II lines, indications of pronounced magnetic activity may be able to determine activity cycles and thus assist in predetermining conditions prone to produce energetic flares.

Lastly, this method may be suitable for small observatories provided careful measurement techniques are used combined with rigorous data analysis

and signal processing techniques. The benefit of the FIR filter signal processing is that the flare profile can be matched through the light curve in the midst of background flickering, noise, and sympathetic flaring. During superflare events, the flickering and sympathetic flaring tend to occur at much lower amplitudes and therefore consist of different profile characteristics. Therefore, the FIR filter will tend to ignore the unmatched flaring, given a high enough time resolution in the flare profile. This will serve to reduce the effective  $\varepsilon$  attainable for a given observatory, potentially affording observations of faint echoes.

#### Limitations of the Echo Detection Method

As noted previously, one limitation of the echo method is that the flare duration is much shorter than the light travel time from the star to the planet. If the light travel time to the planet is less than or nearly equal to the flare duration, then the echo will not be detectable. Additionally, if the flare is multi-peaked, the unique peak profile must be constrained within the light travel time to the planet.

Like other methods, this method is of limited usefulness when the echo's peak amplitude is close to or below the background noise level. This requires that the planet be large enough, close enough, and has high enough albedo to produce a signal.

The echo detection method will produce a coupled parameterization of the planet coupled to the planets radius, distance from the host star, albedo, orbital inclination, and relative location within the orbit. Since this method cannot uniquely determine any of these characteristics, other methods of detection will be needed to validate these parameters. This method will require other complementary methods, such as spectroscopy or radial velocity measurements.

So far, in the discussion of the method it has been assumed that the flare signal emanates simultaneously from all portions of an entire hemisphere of the star. Another assumption is that the echo emanates from the entire hemisphere of the planet. In contrast for both assumptions, the exact atmospheric conditions for any given flare are unknown. As noted by Gurzadyan (1986), flares produced on the opposite side of the star will also be visible through the stellar chromosphere. The effect however is to exhibit a slower rise time from atmospheric transition. As applied to the flare echo detection method, a slower response time in the flare profile may limit the effective range resolution due to the increase in flare pulse duration.

## OBSERVATIONS

### Selection of Test Cases

In order to develop a list of candidate stars for testing the flare echo detection method, a list of ideal targets was generated. The criteria used for target selection were as follows: 1) The stars are known to exhibit massive flares, 2) the flares are periodic on short timescales compared to a human lifetime, 3) the predicted echo strength is  $< 1 \times 10^{-6}$ , 4) for the orbital inclination is such that the planet passes in between the star and earth's view, called a planet transit, and 5) the star is nearby so that parallax data exist to determine distance. The last two criteria are necessary for validation of experimental results, however are not necessary for the detection mechanism to be useful in practical application.

The most readily accessible sources of information on extrasolar planets are the *Exoplanets Encyclopedia* and the *Transitsearch.org* websites. Using the list of known transiting planets, the Gershberg UV-Cet type flare star catalog (1999) was searched<sup>3</sup> for possible matches. Unfortunately, there were no matches found. A match might be found if the entire list of known extrasolar planets were included, however it is unlikely that this is the case. Due to the typical selection criteria of extrasolar planet searches, especially for radial velocity surveys, stars with this sort of variability are excluded. However, as noted by Robinson et. al. (2007), the selection criteria are now being modified to include different parameters.

The list of superflare stars from Schaefer (2000) and Rubenstein (2001) were included in the targets list. The assumption of 1-Jupiter radius planet at a

---

<sup>3</sup> Using SIMBAD as a name resolver, all starnames were converted the first instance in the following hierarchy: HD, HIP, GSC, BD, other.

distance of 0.05 AU has been taken for a theoretical prediction of  $\epsilon$  leads to a calculated echo strength of  $4.5 \times 10^{-5}$ . These stars were known at least at one time to exhibit a very energetic flare of several orders of magnitude grander than those exhibited by the Sun. These superflare stars thus meet criteria 1 identified previously. The superflare stars were cross-referenced to the *Extrasolar Planets Encyclopedia* and the *Transitsearch.org* databases and no matches were found indicating that these stars are not known for variability.

A further criterion for target selection was the theoretical prediction of a hypothetical star-planet system. Of the list of known extrasolar planets, the planetary radius is plotted against the distance from the parent star (see Figure 12). Where the planetary radius is unknown, the planet's radius is assumed equal to one Jupiter radius. Where the semi-major axis is unknown, the semi major axis is assumed to be 0.05 AU. Where neither value is known, the planet is excluded from the plot. In Figure 12, the lines of constant geometrical echo strength according to Equation 5 are shown.

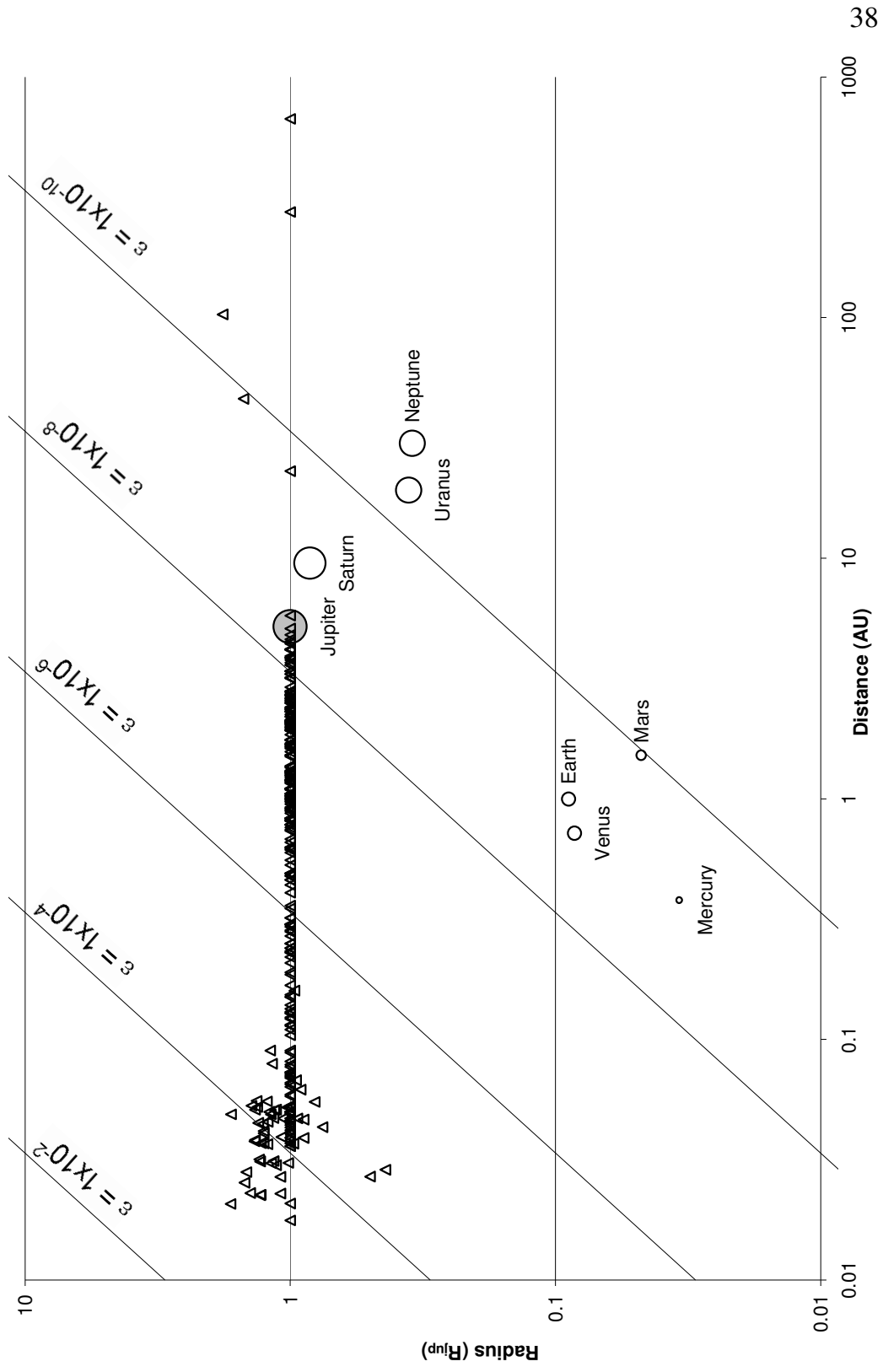


Figure 12. Theoretical Echoes From Known Solar (O) and Extrasolar (Δ) Planets Using geometrical Model.

The selection criterion #3 for the list of target stars begins with the stars that have the highest predicted echo strength according to Figure 12. The cutoff used for the selection process was extended to  $\epsilon > 6 \times 10^{-5}$ . Next, the combined list of superflare stars from Schaefer (2000) and Rubenstein (2001) was included. An additional criterion for selection was purely for observability from mid-northern latitudes. Those stars with declination below  $-35^\circ$  were excluded from the candidates list. The final criterion for the initial targets list is the ability to observe the target between November and May.

The seasonal observability tables were created using Skycalc (Thorstensen, 2007). The observability times are based on dual criteria; that the object is observable for at least one hour per night and at air mass  $> 2.0$ . The initial targets list, an activity indication, and the predicted echo strengths are summarized in Table 5.

Table 5. List of Candidate Stars and Hypothetical Echo Strengths.

<b>Resolved Name</b>	<b>Starname</b>	<b>Active</b>	<b><math>\epsilon</math> (<math>\times 10^{-6}</math>)</b>
<i>Stars with known extrasolar planets</i>			
GSC 04804-02268	CoRoT-Exo-1		39.1
GSC 03089-00929	TrES-3		37.3
GSC 00465-01282	CoRoT-Exo-2		30.9
GSC 05819-00957	GL 876	X	26.2
GSC 02636-00195	WASP-3		19.4
HD 189733	HD 189733	X	15.6
GSC 03547-01402	HAT-P-7		14.8
GSC 02265-00107	WASP-1		14.4
GSC 02752-00114	WASP-10	?	13.7
GSC 02620-00648	TrES-4		13.4
GSC 01482-00882	WASP-14	?	13.2
GSC 03549-02811	TrES-2		12.6
GSC 00522-01199	WASP-2		12.5
GSC 02634-01087	HAT-P-5		10.9
HD 209458	HD 209458	X	9.8
GSC 02569-01599	HAT-P-4		9.2
GSC 02652-01324	TrES-1		8.6
GSC 03727-01064	XO-3		8.2
GSC 02463-00281	HAT-P-9	?	7.9
GSC 03413-00005	XO-2		7.9
HIP 57087	GJ 436	X	2.6
<i>Superflare stars</i>			
HD 103095	Groombridge 1830		45
HD 136202	5 Serpentis		45
HD 137050	UU Corona Borealis		45
HD 1522	i Cet		45
HD 187691	Omicron Aquilae		45
HD 20630	Kappa Ceti		45
HD 23686	S Fornacis		45
HD 72905	Pi1 Ursae Majoris		45
HIP 73707	BD + 10°2783		45

The activity indication in Table 5 above denotes with an “X” stars that have shown X-Ray activity as reported by Kashyap, et. al. (2008). A question mark denotes those stars for which no information was available. The presence of X-Ray activity in a star with known extrasolar planets is not unique. However, since the identified stars have X-Ray flux differing from the expected flux, these stars would be good candidates for further investigation.

### Observational Data

Once the targets list was defined, observing time at California State University Fresno’s Sierra Remote Observatory (SRO) became a problem: bad weather over the entire observing window from October to March placed a significant barrier to obtaining data. Therefore, time resolved photometric observations of only one target star were taken during autumn of 2008. The choice of particular target star was primarily because of all the superflare stars, this star had listed the highest observed flare energy. S Fornacis was therefore chosen because of its high probability of detecting an echo should one occur in the dataset. The data for were taken on 2008-11-29, 2008-12-02, 2008-12-4, and 2008-12-5 by Dr. Frederick Ringwald from SRO and analyzed by the author. The analysis of the photometry data is summarized below.

Data analysis was performed using the AIP4WIN version 2 differential photometry measurement tool. For the first two nights, the images were taken from SRO using a 16” Schmidt-Cassegrain telescope at f/8 using an SBIG STL-11000M camera binned 3x3 through a blue filter with 5 second exposures. For the remaining two nights, the images were binned 9x9 with 1 second exposures. Images were calibrated using the advanced calibration with Bias, Dark, Flat, and Flatdark calibration frames, median combined, and applied to each image. The

photometric annulus was drawn at 7 pixels with sky ring set between 10 and 15 pixels. During the first two nights, several images had visual defects presumably due to process buffering during image readout. These images were discarded from evaluation.

The stars chosen for the comparison stars are noted in Table 6 and the associated type I (statistical) measurement errors are shown in Table 7. The errors from the second two nights are higher than those of the first two due to the exposure time used.

Table 6. Information on S Fornacis and Comparison Stars Used in Time Resolved Photometry Measurements.

ID	Target Name (and alternates)	Comments
V	S Fornacis, HD23686 GSC 06448-01068	G1V star with B = 9.2 (parallax = 6.81 mas)
C1	HD 23755 GSC 06448-00954	G3V star with B = 10.29
C2	HD 23815 GSC 06448-00876	K4III star with B = 10.34
C3	TYC 6448-1073-1 GSC 06448-01073	Unknown spectral type with B = 11.9 (B-V = 1.5)
C4	CD-24 1854, GSC 06448-01103	G5 star with B = 11.3

Table 7. S Fornacis Measurement Error Statistics

Measurement	First two nights		Second two nights	
	Maximum Error	Average Error	Maximum Error	Average Error
V-C1	0.016	0.008	0.097	0.030
C1-C2	0.049	0.015	0.174	0.085
$V_{\text{ens}}$	0.011	0.006	0.093	0.029

A graphical representation of the data presented sequentially is shown below in Figure 13. Analysis of the present data taken of S Fornacis shown in Figure 13 demonstrates that a superflare event was not observed above the

measured noise level. Tests for statistical significance in the low-level fluctuations of the variable star demonstrate some contribution from shot noise (random noise due to lack of photons) and some contribution from scintillation noise (fluctuations in the refractive index of the atmosphere). There exists some statistical evidence of noise that can be neither attributed to shot noise nor scintillation noise; this may stem from rapid variability in the atmosphere of S Fornacis, which would represent evidence of microflaring or flickering (Schaefer, 2009). Rapid stellar variability in the dataset is unexpected and inconsistent with the age and spectral type of the star. Further observations would be necessary to confirm this.

Note the relative differential photometry values for each measurement,  $V-C1$ ,  $C1-C2$  and  $V_{ens}$  have all been adjusted by fixed values for easy comparison on the same graph.

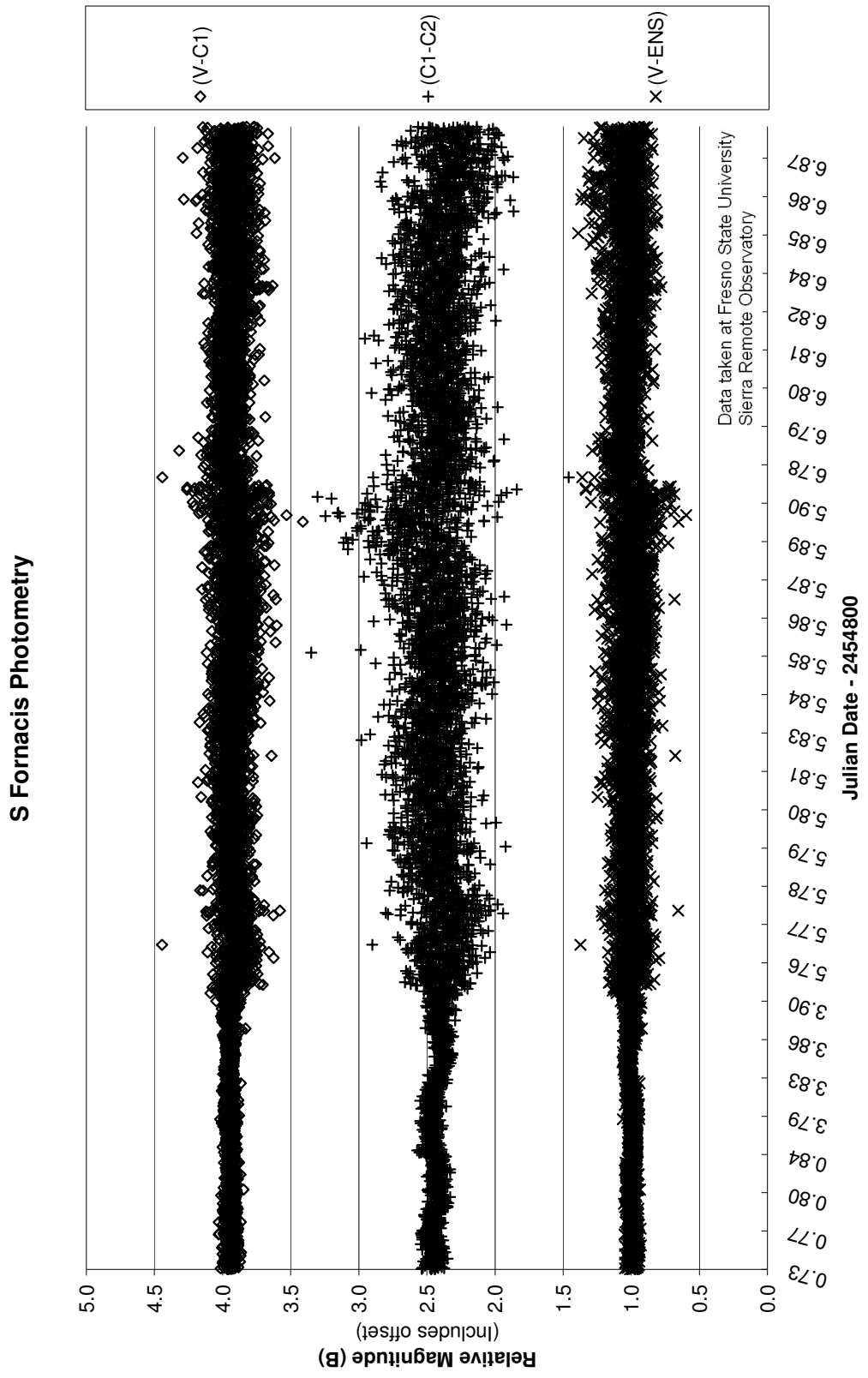


Figure 13. Photometric Data of S Fornacis (No Observed Superflares).

## EXPOSITION

The detection of a planet by flare echoes has yet to be successfully accomplished. The theoretical groundwork demonstrates a high probability that the method has merit and should be investigated further. The list of candidate stars in Table 5 provides a starting point for further observations. It is likely that the method may prove useful for small observatories, such as Fresno State's Sierra Remote Observatory.

Enhanced chromospheric activity has already been observed due to the magnetic field interactions of stars with nearby giant planets (Lanza, 2008; Kashyap, et. al., 2008). The degree to which this magnetic interaction may stimulate stellar flares or even superflares remains an open question.

With the planned new observatories designed for long-term all sky surveys, energetic stellar flares may be more readily identifiable. With the knowledge and characterization of flare stars, the viability of this detection method may soon become more attractive. As the population and variety of known extrasolar planets continues to expand, so does the likelihood of validation for this detection method.

## REFERENCES

## REFERENCES

- Azary, Zoltan. Personal Interview. 2009 Feb. 20.
- Böhm-Vitense, Erika. Introduction to Stellar Astrophysics. Volume 2: Stellar Atmospheres. New York: Cambridge University Press, 1997.
- Bromley, Benjamin C. “Detecting Faint Echoes in Stellar-Flare Light Curves.” Publications of the Astronomical Society of the Pacific. 104 (1992): 1049-1053.
- Berry, Richard and James Burnell. The handbook of astronomical image processing. 2<sup>nd</sup> ed. Richmond: Willmann-Bell, 2005.
- Byrne, Patrick B. and Marcello Rodonò. Eds. Activity in Red-Dwarf Stars: Proceedings of the 71<sup>st</sup> Colloquium of the IAU, Catania, Italy, 1982 August 10-13. Boston: D. Reidel Publishing Company, 1983.
- Byrne, Patrick B. “Giant starspots and stellar flares: the view from space.” Irish Astronomical Journal. 18 (1988): 172-176.
- Comins, Neil F. and William J. Kaufmann III. Discovering the Universe. New York: WH Freeman and Company, 2005.
- Cranmer, Steven R. and Steven H. Saar. “Exoplanet-Induced Chromospheric Activity: Realistic Light Curves from solar-Type Magnetic Fields.” Preprint [astro-ph]. 2007. arXiv: 0702530v1.
- Cuntz, Manfred, Steven H. Saar and Zdzislaw E. Musielak. “On stellar activity enhancement due to interactions with extrasolar planets.” Astrophysical Journal. 533 (2000): L151-L154.
- Dimitrov, D. P. and K. P. Panov. “The flare activity of YZ CMi in 1999-2004.” Aerospace Research in Bulgaria, 2006. Online Internet. Available [www.space.bas.bg/astro/Rogen2004/StPh-10.pdf](http://www.space.bas.bg/astro/Rogen2004/StPh-10.pdf)
- Dorf, Richard C. The Electrical Engineering Handbook. Boca Raton: CRC Press, 1993. Ch 39.
- Extrasolar Planets Encyclopedia. Online internet. Available [exoplanet.eu](http://exoplanet.eu)

- General Catalog of Variable Stars (GCVS). Online internet. Available [www.sai.msu.su/groups/cluster/gcvs](http://www.sai.msu.su/groups/cluster/gcvs)
- Gershberg, Roald E. Solar-Type Activity in Main-Sequence Stars. New York: Springer, 2005.
- Gershberg, Roald E. et. al. “Catalogue and bibliography of the UV Cet-type flare stars and related objects in the solar vicinity.” Astronomy & Astrophysics Supplement Series. 139 (1999): 555-558.  
Online internet. Available [heasarc.nasa.gov/W3Browse/all/flarestars](http://heasarc.nasa.gov/W3Browse/all/flarestars).
- Greiner, Jochen, Hilmar W. Duerbeck and Roald E. Gershberg. Eds. Flares and Flashes: Proceedings of IAU Colloquium No. 151 held in Sonneberg, Germany, 1994 December 5-9. New York: Springer, 1995.
- Gurzadyan, G. A. “Flares on opposite sides of the star: Observational Aspects.” Astrophysics and Space Science. 129 (1986): 127-147.
- Haisch, B. M. and M. Rodonò. Eds. Solar and Stellar Flares: Proceedings from IAU colloquium 104. Catania Astrophysical Observatory Special Publication. 1989: 53.
- Haisch, Bernhard, Keith T. Strong and Marcello Rodonò. “Flares on the Sun and other stars.” Annual Review of Astronomy and Astrophysics. 29 (1991): 275-324
- Harvey, A. F. Microwave Engineering. London: Academic Press, 1963. Ch 25.
- Henden, Arne A and Ronald H. Kaitchuck. Astronomical Photometry. New York: Van Nostrand-Reinhold, 1982.
- Kashyap, Vinay L., Jeremy J. Drake and Steven H. Saar. “Extrasolar Giant Planets and X-Ray Activity.” The Astrophysical journal. 687(2008): 1339-1354.
- Lanza, A. F. “Hot Jupiters and stellar magnetic activity.” Astronomy & Astrophysics. Preprint [astro-ph]. 2008. arXiv: 0805.3010v1.
- Lanza, A. F. et al. “Photospheric activity and rotation of the planet-hosting star CoRoT-Exo-4a” Preprint [astro-ph]. 2009. arXiv: 0901.4618v1.
- Martens, P. C. H. and N. P. M. Kuin. “A circuit model for filament eruptions and two-ribbon flares” Solar Physics. 122 (1989): 263-302.

- Robinson, Sarah E. et. al. “The N2K consortium. VII Atmospheric Parameters of 1907 metal-rich stars: Finding planet-search targets.” Astrophysical Journal Supplement Series. 167 (2007): 430-438.
- Rowe, Jason F. et. al. “The Very Low Albedo of and Extrasolar Giant Planet: MOST Spacebased Photometry of HD 209458b.” The Astrophysical Journal. 286 (2008): 1345-1353.
- Rubenstein, Eric P. “Superflares and Giant Planets.” American Scientist. Jan. – Feb. 2001:38-45.
- Rubenstein, Eric P., Bradley E. Schaefer. “Are superflares on solar analogues caused by extrasolar planets.” The Astrophysical Journal. 529 (2000): 1031 – 1033.
- Saar, Steven H. Letter to the author. 9 March 2009.
- Saar, Steven H. and Manfred Cuntz. “A search for Ca II emission enhancement in stars resulting from nearby giant planets.” Monthly Notices of the Royal Astronomical Society. 325 (2001): 55-59.
- Schaefer, Bradley E. Letter to the author. 8 March 2009.
- Schaefer, Bradley E., Jeremy R. King and Constantine P. Deliyannis. “Superflares on ordinary solar-type stars.” The Astronomical Journal. 529 (2000): 1026-1030.
- SIMBAD Astronomical Database. Online internet. Available [simbad.harvard.edu/simbad](http://simbad.harvard.edu/simbad).
- Schrijver, Carolus J and Cornelis Zwaan. Solar and Stellar Magnetic Activity. New York: Cambridge University Press, 2000.
- Shkolnik, Evgeny et. al. “Star-Planet Interactions.” Preprint [astro-ph]. 2008. arXiv: 0809.4482v1.
- Shkolnik, Evgenya et. al. “The on/off nature of Star-Planet interactions.” Preprint [astro-ph]. 2004. arXiv:0712.0004v1.
- Smith, J.O. Introduction to Digital Filters with Audio Applications. Online book. 21 Feb. 2009. Available [ccrma.stanford.edu/~jos/filters/](http://ccrma.stanford.edu/~jos/filters/).

- Spangler, Steven R. and Thomas J. Moffett. "Simultaneous Radio and Optical Observations of UV Ceti-Type Flare Stars." The Astrophysical Journal. 203 (1976): 497-508.
- Sugerman, Ben E. K. "Observability of scattered-light echoes around variable stars and cataclysmic events." The Astronomical Journal. 126 (2003): 1939-1959.
- Thorstensen, John. Skycalc. Computer Software. Astronomical almanac calculator. Modified by Frederick Ringwald, 2007. DOS/Windows. 457KB. Download. Online Internet. Available [zimmer.csufresno.edu/~fringwal/skycalc](http://zimmer.csufresno.edu/~fringwal/skycalc)
- Transitsearch. Online. Available [www.transitsearch.org](http://www.transitsearch.org).
- Zombeck, Martin V. Handbook of Astronomy and Astrophysics. Cambridge: Cambridge University Press, 1990. 2<sup>nd</sup> ed.